Journal of Alloys and Compounds 479 (2009) 511–519

Contents lists available at ScienceDirect

Journal of Alloys and Compounds

journal homepage: www.elsevier.com/locate/jallcom

Structural and morphology comparison between m-$LaVO_4$ and $LaVO_3$ compounds prepared by sol–gel acrylamide polymerization and solid state reaction

G. Herrera[a,*], E. Chavira[b], J. Jiménez-Mier[c], A. Ordoñez[b], E. Fregoso-Israel[b], L. Baños[b], E. Bucio[c], J. Guzmán[b,d], O. Novelo[b], C. Flores[b]

[a] Posgrado en Ciencias Químicas, Universidad Nacional Autónoma de México, Circuito Exterior s/n, 70-360, 04510 México D.F., Mexico
[b] Instituto de Investigaciones en Materiales, Universidad Nacional Autónoma de México, 70-360, 04510 México D.F., Mexico
[c] Instituto de Ciencias Nucleares, Universidad Nacional Autónoma de México, 70-543, 04510 México D.F., Mexico
[d] Centro de Investigación en Ciencia Aplicada y Tecnología Avanzada, Instituto Politécnico Nacional 11500 México D.F., Mexico

ARTICLE INFO

Article history:
Received 28 October 2008
Received in revised form
22 December 2008
Accepted 23 December 2008
Available online 19 January 2009

Keywords:
Ceramics
Sol–gel processes
Microstructure
Atomic force microscopy (AFM)
X-ray diffraction

ABSTRACT

We contrast the production of $LaVO_3$ polycrystalline samples obtained by reduction of m-$LaVO_4$ prepared by sol–gel acrylamide polymerization (SGAP) and solid state reaction (SSR). For SGAP the formation of m-$LaVO_4$ occurs at 400 °C, for SSR at 1400 °C. For m-$LaVO_4$-SGAP we observe a homogeneous morphology with needle-shaped grains of 50 nm average size. The SSR presents a broader size distribution in the micrometer range. Both m-$LaVO_4$ samples were reduced into $LaVO_3$ using a Zr rod at 850 °C in vacuum. $LaVO_3$-SGAP presents a homogeneous grain distribution with an average size of 745 nm. $LaVO_3$-SSR has an average size of 3.45 μm. The stoichiometry of all compounds was confirmed by energy dispersive X-ray spectroscopy. X-ray powder diffraction and transmission electron microscopy give crystal structures in agreement with those reported in the literature.

1. Introduction

$LaVO_4$ and $LaVO_3$ are lanthanum orthovanadates that belong to a group of compounds with interesting structural, electronic, magnetic and electrical properties at low temperatures [1–4].

The crystal structure of $LaVO_4$ compound has been reported in two polymorphs, namely, tetragonal zircon-type (t-$LaVO_4$) [5] with D_{4h}^{19} [6] $I4_1/amd$ (No. 141) space group isostructural to $ZrSiO_4$ compound [7,8] and monoclinic monazite-type (m-$LaVO_4$) with C_{2h}^5 $P2_1/m$ (No. 11) space group [9] whereas [10,11] reported it to be monoclinic with $P2_1/n$ (No. 14) space group, isostructural to $CePO_4$ compound. Andreeta et al. [12] reported at temperatures above 300 °C it has a structural transition from tetragonal ($I4_1/amd$) to monoclinic ($P2_1/n$). Generally, with increasing ionic radius, Ln^{3+} ions show a strong tendency toward monazite-structured orthovanadate due to its higher oxygen coordination number of 9 [10] as compared with 8 of the zircon one [13]. For this reason $LaVO_4$ chooses monazite type as the thermodynamically stable state while the other orthovanadates normally exist in the zircon type [13].

$LaVO_3$ compound has an orthorhombic distorted perovskite structure with the D_{2h}^{16} [14] Pnma (No. 62) space group first found in $GdFeO_3$ compound [15–19]. An interesting phenomenon in this compound is the phase transition from orthorhombic to monoclinic structure at about 140 K. It is accompanied by a paramagnetic to antiferromagnetic transition [20–26]. Because of their intrinsic characteristics lanthanum vanadates have recently gained interest due to their surface catalytic properties and binary oxides of vanadium have been proposed as catalysts for vapour phase dehydrogenation of propane, butane, ethylbenzene and parafins [27–30]. Also, they can be used as polarizers [31] laser host materials [32] and luminescent materials [33–37], phosphors [38,39] and solar cells [40].

The common method to prepare polycrystalline samples is the solid state reaction (SSR). It presents some disadvantages. It is time-consuming, it needs high temperatures (>1000 °C) [18,41] and multiples repetitions of thermal treatments to achieve the chemical reaction. It produces an inhomogeneous grain size distribution in the micrometer scale (1–10 μm). It also results in an inhomogeneous chemical composition [42]. $LaVO_4$ and $LaVO_3$ compounds have been produced by solid state reaction with different heat treatments with temperatures greater than 1000 °C to achieve the chemical reaction [11,15,16].

* Corresponding author.
E-mail address: guillermo.herrera@nucleares.unam.mx (G. Herrera).

0925-8388/$ – see front matter © 2009 Elsevier B.V. All rights reserved.
doi:10.1016/j.jallcom.2008.12.146

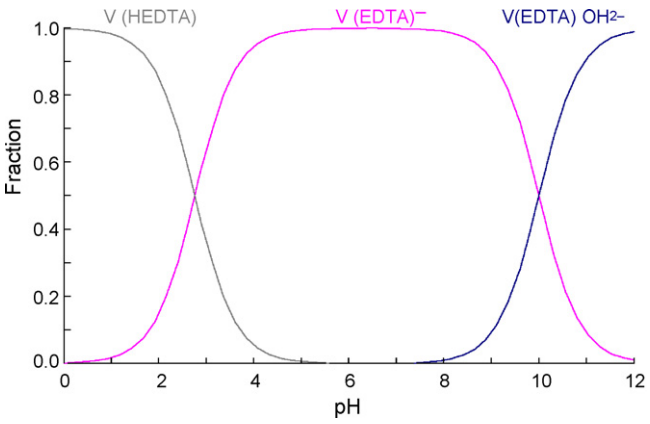

Fig. 1. Speciation diagrams for vanadium as a function of pH for the 1:1 metal:EDTA molar ratio.

Fundamental research requires very pure and high quality samples with single phase compounds. One of the most promising ways to obtain an excellent homogenization at an atomic scale of the elements and a high reactivity of the precursor is the sol–gel acrylamide polymerization (SGAP) [43]. The resulting powders show a homogeneous grain size distribution in the nanometer range [43]. This synthesis method is fast, clean and easy to reproduce with the advantage of a reduction in the temperature to complete the chemical reaction [44–48]. Recently, this method was used to control the grain size homogeneity [49] and which also improve thermoelectric properties of samples [50].

In this work, we compare the fabrication of $LaVO_3$ compounds obtained by reduction of $LaVO_4$ compound prepared by SGAP and SSR. We then compare the effects of both synthesis methods in the morphology and grain size distribution.

2. Experimental procedure

2.1. Sol–gel acrylamide synthesis, SGAP

2.1.1. Materials

La_2O_3 (CERAC, 99.99%) and V_2O_5 (CERAC, 99.9%); HNO_3 (J.T. Baker, 69–70%); ethylenediamine tetraacetic acid, EDTA $[CH_2N(CH_2CO_2H)_2]_2$ (Fluka, 99%); NH_4OH (J.T. Baker, 28–30%); acrylamide, $H_2C{=}CHCONH_2$ (Fluka, 99.9%); N,N′-methylene bisacrylamide, $C_7H_{10}N_2O_2$ (Fluka, 99.5%) and α,α′-azodiisobutyramidine dihydrochloride, AIBN, $C_8H_{18}N_6{\cdot}2HCl$ (Fluka, 98%) were used in the fabrication of $LaVO_4$ by SGAP.

2.1.2. Sol formation

A 50 mol% of stoichiometric proportion of La_2O_3 compound was completely dissolved in 150 ml of distilled water with 3–5 ml of HNO_3 to obtain a transparent solution of $La(NO_3)_3$ and 50 mol% of V_2O_5 was dissolved in H_2O_2 (this agent was used to increase the reaction speed) with 3–5 ml of HNO_3 to obtain 2 g of the sample. To increase the dissolution velocity and its homogeneity the resulting dissolution was mixed at 90 °C in a magnetic stirrer (Ika CERAMAG model Mid).

2.1.3. Gel formation

Each sol was mixed with the chelating agent, EDTA, using the molar ratio (M:EDTA 1:1), where M is the metal in the sol. EDTA combines with metal ions to form stable chelates, in a 1:1 ratio regardless of the charge on the cation [51]. The pH of the solution can influence the metal speciation, precipitation and the protonation degree. Concentration of EDTA influences on the degree of metal complexation and subsequently the concentration of free metal in solution [52]. Fig. 1 shows the species distribution diagram as a function of pH, calculated by MEDUSA computer program [53], for solution of 1:1 vanadium–EDTA molar ratio. The graph indicates than 100% of vanadium is complex as metal–EDTA specie in the pH region of 2.75–10. We used this chelating agent to encapsulate the rare earth element $La^{(3+)}$ and the transition element $V^{(5+)}$ metals ions. The mixture was kept at 80–90 °C under constant stirring. This step is designed to prevent the ions from forming complexes until the "in situ" reactions start. The ions then keep their stability during the decomposition of EDTA. The reactions for each cation in this step are

$$La_2O_3 + H_2O + 6HNO_3 \rightarrow 2La(NO_3)_3(\text{whitetransparentsolution}) + 4H_2O\uparrow \quad (1)$$

$$4La(NO_3)_3 + [CH_2N(CH_2CO_2H)_2]_2 + H_2O \rightarrow [CH_2N(CH_2CO_2La)_2]_2 + 4HNO_3 + H_2O + 12O_2 + 4N_2\uparrow \quad (2)$$

$$V_2O_5 + H_2O_2 + 6HNO_3 + H_2O \rightarrow 2VO(NO_3)_3(\text{green–yellowtransparentsolution}) + 5H_2 + 3O_2\uparrow \quad (3)$$

$$4VO(NO_3)_3 + [CH_2N(CH_2CO_2H)_2]_2 + H_2O_2 \rightarrow [CH_2N(CH_2CO_2V)_2]_2 + 12HNO_3 + H_2O\uparrow \quad (4)$$

The generation of $VO(NO_3)_3$ [54] and their stability in nitric acid solutions and its persistence even in the presence of water was reported by Logan [55]. After this step the pH value was 0.63. The solution was then mixed, with 10–20 ml of NH_4OH in order to adjust the pH to 5.4 because the fast acrylamide polymerization proceeds generally in aqueous medium whose pH is close to neutral [43,52]. This process was performed at room temperature. To the solution (300 ml) we added a 10 wt.% of $H_2C{=}CHCONH_2$ monomers to start the polymerization [43] and to accelerate the gel formation. We added 2 wt.% of the cross-linker, $C_7H_{10}N_2O_2$. Also 1 wt.% of $C_8H_{18}N_6{\cdot}2HCl$ is added to regulate the weight of acrylamide and to increase the velocity of interconnections. The thermopolymerization process was carried out under continuous magnetic stirring at 80 °C for 12 min until an opaque yellow viscous gel is produced.

2.1.4. Xerogel formation

We obtained the desiccate gel (xerogel) under an Ar atmosphere using a microwave oven (SEV-MIC IV) after 30 min operating at 600 W. This xerogel was grinded in an agate RM 100 mortar (model Retsch), and the powder was heated first to 200 °C during 12 h. Next we increased the temperature in 100 °C steps up to 400 °C in a thermolyne 46100 furnace maintaining the temperature during 12 h in each step. In this stage important organic and amorphous materials are removed and nanocrystals are grown as we will discuss in Section 4. The temperature was increased at a rate of 5 °C/min. At the end of the synthesis we obtained 96% (1.92 g) of the sample. The mixture was then compacted into pellets (diameter 13 mm thickness 1.0–1.5 ± 0.05 mm) exerting a pressure of 4 ton/cm^2 in an Press (Osyma) for 3 min under vacuum.

2.2. Solid state reaction synthesis, SSR

La_2O_3 (CERAC, 99.99%), V_2O_5 (CERAC, 99.9%) and ethanol (J.T. Baker, 70%) were used in the fabrication of polycrystalline lanthanum vanadate by SSR.

In this technique, raw materials La_2O_3, and V_2O_5 were weighted, mixed with ethanol and milled during 15 min in an agate mortar to form a slurry. The milled powder was heated at 800 °C in a thermolyne 46100 furnace (±4 °C) during one day in air. The resulting material was compressed into pellets (diameter 13 mm thickness 1.0–1.5 ± 0.05 mm) exerting a pressure of 4 ton/cm^2 for 15 min under vacuum.

2.3. Reduction of samples

The single phase of $LaVO_4$ powders prepared by both synthesis methods were compacted into pellets and then reduced with a metallic Zr rod (Aldrich 99%). Each sample and a metallic Zr rod were enclosed in a quartz tube in vacuum. The temperature was kept at 850 °C during 15 days. After this period of time the sample was quenched in ice. In this step one can observe the oxidation of metallic Zr rod. The choice of metallic Zr as a gatherer [56] is justified by looking at the thermodynamic stabilities and the standard Gibbs energies of formation $\Delta G^{\circ}_{f,\ ox}$ of $LaVO_4$ and $LaVO_3$ compounds [29,57,58] and of metallic Zr and ZrO_2 [59]. The reaction could be represented by the following equation:

$$2LaVO_4 + Zr \rightarrow 2LaVO_3 + ZrO_2 \quad (5)$$

3. Characterization techniques

An atom force microscope AFM (JSPM-4210) equipped with tip NSC151SI3N4 with a nominal radii <10 nm, a cantilever strength constant of 40 N/m and frequency constant of 325 kHz in tapping mode was used to investigate the surface morphology, particle size and porosity of the desiccate gel obtained by SGAP. The particle size distribution and the roughness were measured by means of AFM according to three parameters: the standard deviation of the *Z* ranges (RMS), the arithmetic average of the absolute values of the surface height deviations measured from the mean plane (Ra) and peak-to-valley difference in height values (*Z* range). All parameters were analyzed with the WinSPM software [60].

In order to determine the temperature interval in which the reaction should be carried out thermogravimetric (TGA) was performed using Hi-Res 2950 TGA (TA Instruments) and differential thermal (DTA) measurement was obtained in a 2910 DTA with DTA 1600 cell (TA instruments). TGA was used to evaluate the thermal decomposition of the samples prepared by both SGAP and SSR. DTA was used to follow the thermal transformations such as decomposition, phase transformation, polymorphism, melting point, degradation temperatures, purity, chemical stability, volatilization of organic material, etc. of samples. The gel and xerogel obtained by SGAP and reagent mixture prepared by SSR were placed in platinum crucibles and heated starting at room temperature and up to 1000 °C. The heating rates to obtain DTA and TGA were 10 °C/min under a N_2 atmosphere. Also, we obtained DTA spectra for $LaVO_4$ powders prepared by RES and SGPA to follow the transformation of $LaVO_4$ compound into $LaVO_3$ compound. These DTA results were obtained up to 1000 °C with heating rates of 10 °C/min under an Ar atmosphere. The spectra were analyzed by universal analysis software [61].

Crystalline phases were identified by XRD, using a Bruker-AXS D8-Advance with Vantec-1 detector diffractometer for $LaVO_4$ and $LaVO_3$ compounds with λ (Cu_K) = 1.5406 Å radiation. This equipment is able to detect up to a minimum of 1% of impurities. Diffraction patterns of $LaVO_4$ compound were collected at room temperature in a range 2–70° with a step size of 0.020° and time per step of 1.2 s. For $LaVO_3$ compound the XRD pattern was collected at room temperature between 5° and 80° with a step size of 0.017° and time per step of 158.8 s.

The change in morphology of the $LaVO_3$ compound was investigated by scanning electron microscopy, SEM, on a Cambridge-Leica Stereoscan 400. The micrographs were taken between 2.5k× and 5.00k× with a voltage of 20 kV, current intensity of 1000 pA and work distance of 25 mm. The EDX was performed on the same equipment, with an Oxford/Link System electron probe microanalyser (EPMA).

The crystal structure of the $LaVO_3$ compound was studied by TEM with a JEM-1200EXII Jeol microscope. The diffraction patterns were taken with a voltage of 120 kV and a current intensity of 70–80 A, with camera length of 100 cm. The specimens were prepared by dispersing small amounts of powders of the $LaVO_3$ nanocrystals in toluene (Sigma–Aldrich, 99.8%).

To follow the behaviour of functional groups we took the FT-IR spectra for xerogel; powders of $LaVO_4$ compound and powders of $LaVO_3$ compound using a Fourier transform infrared spectrometer Perkin-Elmer PARAGON 5000 in transmission mode. The spectra were analyzed by Spectrum software [62].

Table 1
Mean size of nanometric particles and surface roughness RMS, Ra and *Z* range.

	RMS (nm)	Ra (nm)	*Z* (nm)
Length (nm)			
58.8	7.96	4.76	49.28
Width (nm)			
11.7	2.15	1.58	34.19

4. Results and discussion

4.1. Atomic force microscopy

Fig. 2 shows the AFM results. The morphology and roughness caused by the presence of nanoparticles presented in this topography image reveal needle-shaped particles (needles are made of metal–EDTA and polymer). This crystallization style depends of EDTA molar concentration [63,64] and pH value [65,66]. It has been reported that weak ligand such as EDTA adjusts the morphology and uniformity of crystals shape in the crystallization process. Also, Jia et al. [67] reported that the pH value ranged from 7 to 13 exhibited rods like morphology. The results for the average length, width and roughness are shown in Table 1. The shape and size of particles observed in the surface gel are homogeneous. The needle shape was maintained up to the formation of $LaVO_4$ compound. This result was confirmed by SEM micrographs as we discussed in Section 4.4.1.

4.2. Thermal analysis

To make a comparison of the thermal changes that occurred during synthesis of the samples prepared by SGAP with respect to the samples prepared by SSR, 40.6140 mg of gel and 3.4320 mg of the amorphous xerogel were analyzed by TGA and DTA. The gel and xerogel go through several stages of decomposition upon heating, with overall weight loss of ~95% and 80% respectively. Also 35.6575 mg of the polycrystalline powder of $LaVO_4$ compound prepared by SSR and 36.8458 mg of powders of $LaVO_4$ compound prepared by SGAP were analyzed by DTA.

Fig. 3 shows the thermal behaviour of the gel from 25 °C up to 1000 °C. For purpose of the analysis the TGA and DTA spectra are divided in three regions: 25–200 °C, 200–600 °C and 600–1000 °C.

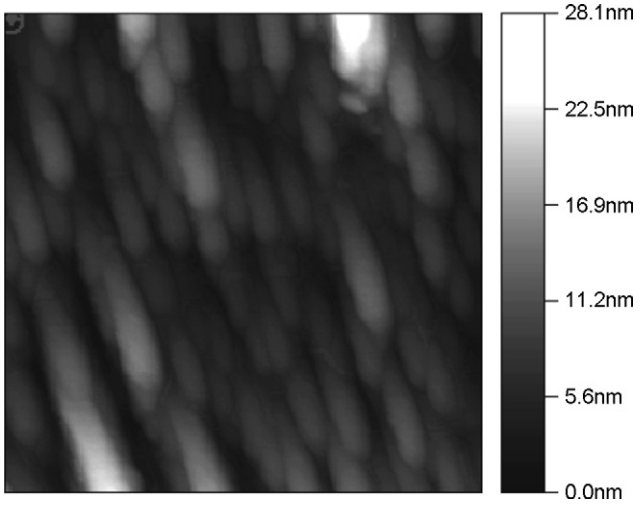

Fig. 2. AFM micrograph obtained by AC mode of gel prepared by SGAP. The image size is 511 nm × 511 nm and clock speed of 666.70 μs.

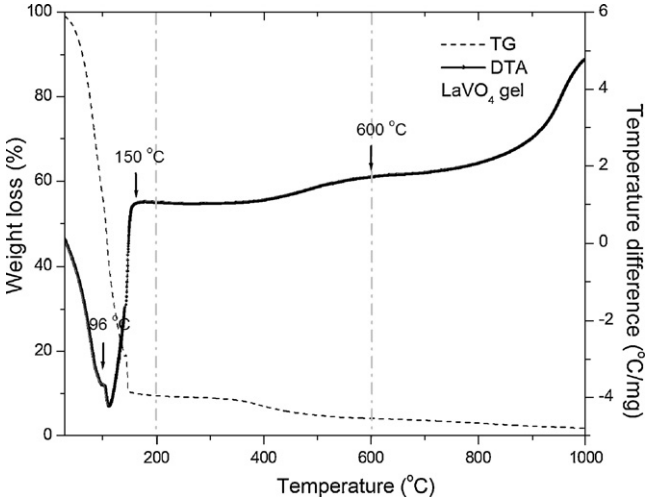

Fig. 3. DTA and TGA for the gel obtained by SGAP at 80 °C during 12 min in a continuous magnetic stirring.

In the first region of TGA one can observe the loss of water and H_2O_2 up to 150 °C. In the next region the loss of weight continues due to the EDTA and organic part denaturalization. In the last region up to 1000 °C one can observe the TGA curve to flatten out above 600 °C indicating complete elimination of all volatile compounds and the organic part. DTA results confirm the TGA results. One can observe two endothermic peaks at 96.9 °C and 133.6 °C due to the evaporation of water and H_2O_2 respectively. An exothermic peak is observed at 161 °C. It is probably due to the break up of EDTA compounds into carbonates and nitrates and the volatilization of NH_4NO_3. At 200 °C the initial formation of $LaVO_4$ compound takes place. In the region between 400 °C and 600 °C one can observe several exothermic variations associated with the decomposition of most of the organic part and release of N_xO_y, CO and CO_2 gases. After 600 °C an increase in the curve means the complete formation of the $LaVO_4$ compound and it represents the thermal stability of nanosized metastable m-$LaVO_4$ due to the small size effects. At ~700 °C we observed a weak endothermic peak may be due to the melting of V_2O_5 (m.p. = 690 °C) [68].

Fig. 4(a) shows the thermal behaviour of the xerogel. TGA and DTA are divided in three regions: 25–200 °C, 200–600 °C and 600–1000 °C. We applied the same criteria to discuss these results. In the TGA one can observe the weight loss at 96 °C and 150 °C due to the dehydration of the precursor.

Between 150 °C and 600 °C the weight loss continues due to the break up of EDTA compounds into carbonates, nitrates and the volatilization of NH_4NO_3 and denaturalization of the organic part. After 600 °C a decrease in the curve means the complete denaturalization of the organic part. In DTA one can observe the exothermal reaction of NO_x group with residuals of the organic part at 248 °C, which is in agreement with the results of Fernández et al. [69]. Also, in this stage La ions have a great chance of reacting with VO_4^{3-} to form $LaVO_4$ nuclei. At around 400 °C (Fig. 4(b)) the complete formation of m-$LaVO_4$ nanocrystals is achieved (this will be discussed when we present the XRD results in the next section). In the region between 600 °C and 1000 °C an increase in the curve means the complete formation of the m-$LaVO_4$ compound.

The decomposition behaviour of the xerogel is completely different to the thermal decomposition behaviour of the gel given in Fig. 4. In the xerogel DTA it was suppress the strong endothermic and exothermic peaks at lower temperatures due to released of gases such as NO_x, H_2O and CO_2 from gel. Compared with conventional oven (12 h at 100 °C as we report in a previous work [49]), the use of microwaves has the advantage of very short reaction favours the phase formation taking place at much lower temperatures. Unfortunately the exact nature of the interaction of the microwaves with the reactants during synthesis of materials is somewhat unclear and speculative [70].

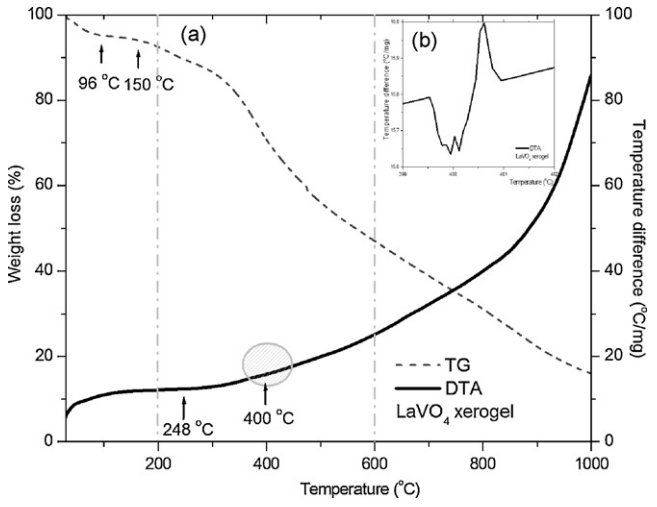

Fig. 4. DTA and TGA for powders of xerogel prepared by SGAP dried in Ar during 30 min in a microwave oven.

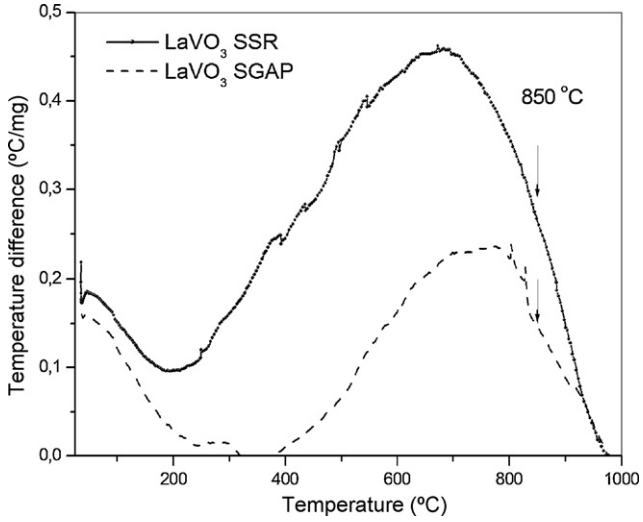

Fig. 5. DTA comparison for powders of m-$LaVO_4$ compound, prepared by SGAP and SSR. At 850 °C one can observe the transformation of m-$LaVO_4$ compound into $LaVO_3$ compound.

In Fig. 5 we present the DTA evolution for nanopowders of m-$LaVO_4$ compound prepared by SGAP at 400 °C during 12 h and powders of $LaVO_4$ compound obtained at 1400 °C at 12 h by SSR in order to determine the crystal transformation to $LaVO_3$ compound. DTA results show that at 850 °C the total transformation of m-$LaVO_4$ compound into $LaVO_3$ compound for both samples. These results would indicate that 850 °C is a useful temperature to establish the heat treatments to reduce the $LaVO_4$ compound into $LaVO_3$ compound.

4.3. X-ray powder diffraction

4.3.1. SGAP

Fig. 6 shows the XRD pattern evolution from the nanocrystalline phase into the $LaVO_4$ crystalline phase prepared by SGAP. Fig. 6(a–c)

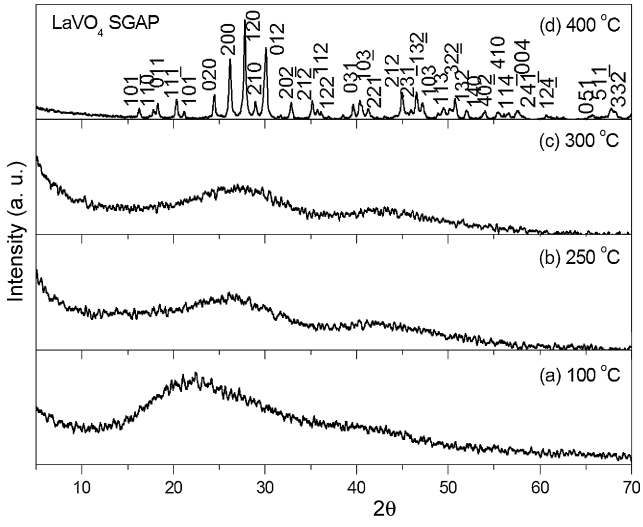

Fig. 6. XRD pattern evolution of $LaVO_4$ compound, prepared by SGAP (a) amorphous phase of xerogel powders, (b and c) at 250–300 °C is still amorphous and (d) at 400 °C single phase pattern related to the m-$LaVO_4$ compound.

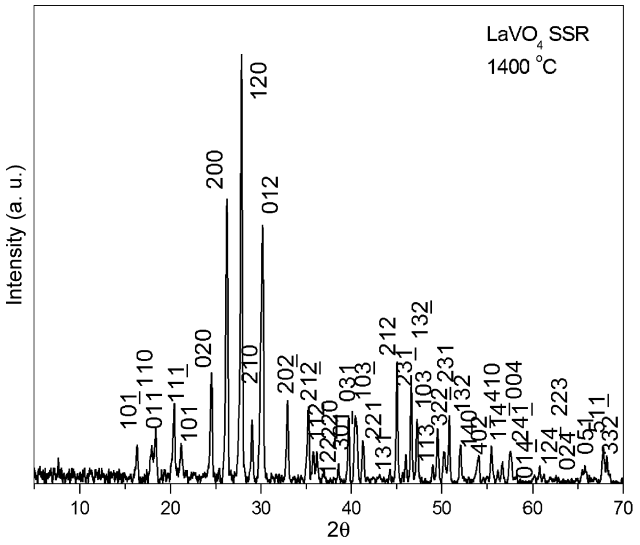

Fig. 7. XRD pattern of m-$LaVO_4$ compound, prepared by SSR kept at 1400 °C during 12 h.

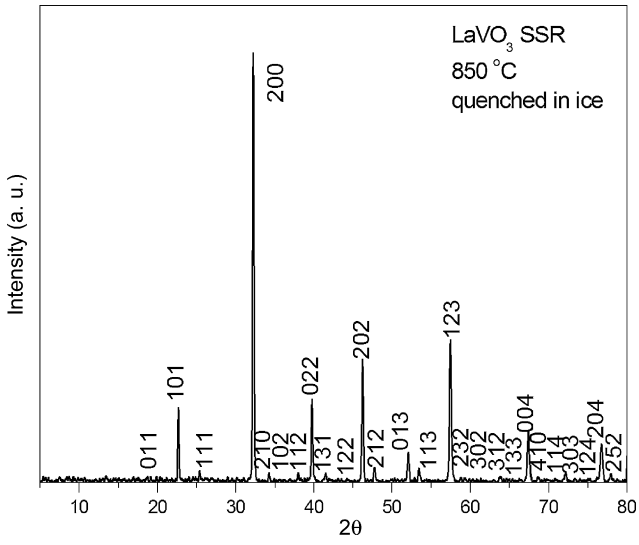

Fig. 8. XRD pattern of $LaVO_3$ compound prepared by SGAP. The sample was enclosed with a metallic Zr rod in vacuum. The heat treatment to reduce the sample was 850 °C during 15 days.

shows a XRD pattern of milled powders of xerogel at 100 °C, 250 °C and 300 °C. These temperatures were maintained during 12 h. The patterns demonstrate the powders are still amorphous. Fig. 6(d) shows the XRD pattern of the powders kept at 400 °C during 12 h. This pattern shows the complete formation of the m-$LaVO_4$ compound. The size of nanocrystallites in m-$LaVO_4$ was calculated using Debye–Scherer formula and determined to lay in the range 23–37 nm. The Debye–Scherer formula is not always a reliable measure of particle size. Hence, other forms of characterization (AFM and TEM) were explored.

At this temperature the reflections are clearly defined, the single phase pattern shows reflections related to the m-$LaVO_4$ compound. This result is in agreement with the phase reported in the powder diffraction file PDF 50-0367 with monoclinic phase and $P2_1/n$ (No. 14) space group [71]. Oka et al. [7] reported that $La(NO_3)_3$ always produced m-$LaVO_4$.

4.3.2. SSR

In Fig. 7 we present the XRD pattern of m-$LaVO_4$ powders prepared by SSR after 12 h of heat treatment at 1400 °C. The single phase pattern shows the reflections of the $LaVO_4$ compound. This result is in agreement with the phase reported in the PDF 50-0367 with monoclinic phase with $P2_1/n$ (No. 14) space group [71].

The widths of the reflections are narrower than the width of the reflection found in the SGAP sample. This means a larger particle size between 349 nm and 563 nm. We conclude here indicating that both $LaVO_4$ samples, obtained by different synthesis procedures crystallize in its thermodynamic state the monazite structure showing the same lattice parameters.

Fig. 8 shows the XRD patterns of powders obtained by SGAP and reduced with metallic Zr to obtain the $LaVO_3$ compound. The particle size determined lay in the range of 35–52 nm.

Fig. 9 shows the XRD for the powders prepared by SSR. The reflections found in these patterns are in agreement with the phase reported in PDF 89-1673 with an orthorhombic phase and Pnma (No. 62) space group [56]. The particle size determined lay in the range of 447–463 nm.

In both cases no other diffraction peaks were observed. The weak presence of ZrO_2 (less than 1%) indicates proper reduction yielding a high-quality product. These results were confirmed by energy dispersive X-rays (see Section 4.4.3).

4.4. Scanning electron microscopy

4.4.1. SGAP

To continue with the study of m-$LaVO_4$ compound we investigate the change in the grain size distribution of samples prepared for both synthesis methods. The micrographs were taken at the surface of powders compacted into a pellet. Grain size and morphology of the sample prepared by both synthesis methods were studied by Carnoy 2.0 version software [72]. The grain size distributions curves allow a determination of the grain size average and its root mean square dispersion using the software Origin 6.0 [73].

We start this analysis with the sample prepared by SGAP. Fig. 10 shows the micrographs of $LaVO_4$ powders at the end of synthesis at 400 °C. We present a micrograph taken at 5.0k× in order to compare the morphology of sample prepared by SGAP with sample obtained by SSR (see Fig. 10(a)), but we show a micrograph (Fig. 10(b)) taken at 25.0k× to better define the grain shape at a nanometer range. It can be seen that the grain size is smaller with grain shape homoge-

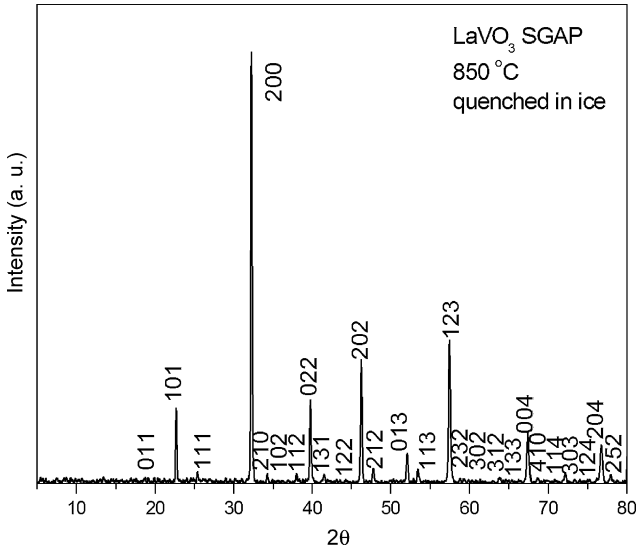

Fig. 9. XRD pattern of $LaVO_3$ compound prepared by SSR. The sample was enclosed with a metallic Zr rod in vacuum. The heat treatment to reduce the sample was 850 °C during 15 days.

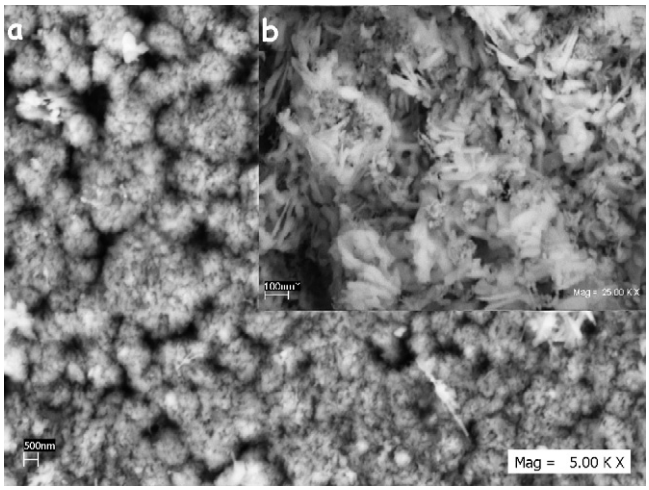

Fig. 10. SEM micrograph of surface of m-$LaVO_4$ compound at the end of synthesis at 400 °C during 12 h in air, prepared by SGAP.

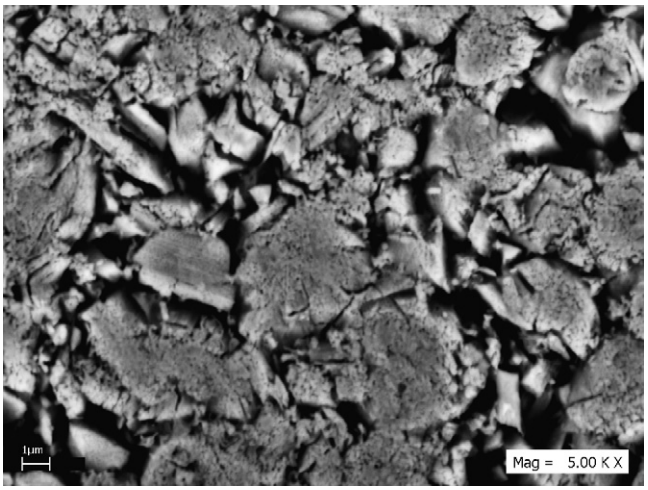

Fig. 12. SEM micrograph of surface of m-$LaVO_4$ compound at the end of synthesis at 1400 °C during 12 h in air prepared by SSR.

neous compared to the sample prepared by SSR presented below. The average size is 123 ± 13 nm.

The morphology presented in this SEM micrograph shows needle-shaped grains. This means that the shape found in the gel (see Fig. 2) is maintained throughout the thermal treatments.

Fig. 11 shows the $LaVO_3$ micrograph on the surface pellet. The pellet was maintained at 850 °C during 15 days in vacuum using a metallic Zr rod as gatherer. One can observe a homogenous grain size distribution with regular shape as a result of the heat treatment. The average grain size is 745 ± 63 nm. It was observed that the grain size shape changed with the transformations of m-$LaVO_4$ compound to $LaVO_3$ compound due to the change of crystal phase. This result is in agreement with XRD pattern. In this step one can corroborate the decrease of oxygen from O_4 to O_3 by EDX (see Section 4.4.3). The optimum temperature to achieve the reduction of the sample is 850 °C.

4.4.2. SSR

Compared to samples obtained by SGPA we find in samples prepared by SSR differences in the morphology and grain size distribution at the end of final reaction temperature. The observed morphology presented in Fig. 12 shows considerable variations in sizes and grain shapes due to the presence of pores. The micrograph was taken at 5.0k× on the surface pellet of the m-$LaVO_4$ sample. We chose this magnification to better define the grains on a larger scale. The sample was heated to 1400 °C during 12 h in air in order to obtain the m-$LaVO_4$ compound. In contrast to the sample prepared by SGAP, this micrograph reveals that for the SSR sample the grain sizes are less homogeneous in shape and size. We determined an average grain size centered in 2.17 ± 0.71 μm.

Fig. 13 shows the micrograph of $LaVO_3$ compound obtained by SSR and maintained at 850 °C during 15 days in vacuum using a metallic Zr rod as gatherer. This heat treatment was chosen in order to keep the same temperature and time conditions of grain growth for both synthesis methods. Time was not sufficient to improve the grain growth as can be seen in this micrograph. The final grain size was 3.15 ± 0.50 μm. Also, one can observe a little improvement in the uniformity of the grain size distribution. The shapes of some grains are similar with the grains observed in Fig. 10 but at different size. These SEM results for both SSR and SGAP samples indicate that the optimum formation of high-purity fine grain size $LaVO_3$ compound is 850 °C.

4.4.3. Energy dispersive X-rays

Global EDX results for m-$LaVO_4$ compound prepared by SGAP and SSR are presented in Table 2. EDX were taken on the surface

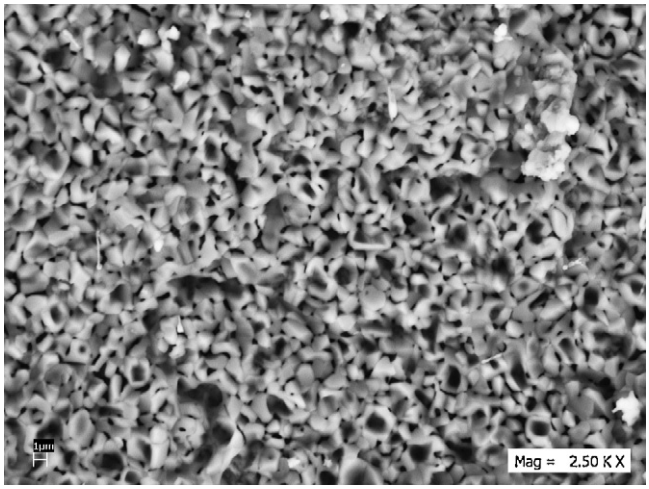

Fig. 11. SEM micrograph on surface of $LaVO_3$ compound at the end of heat treatment at 850 °C during 15 days prepared by SGAP.

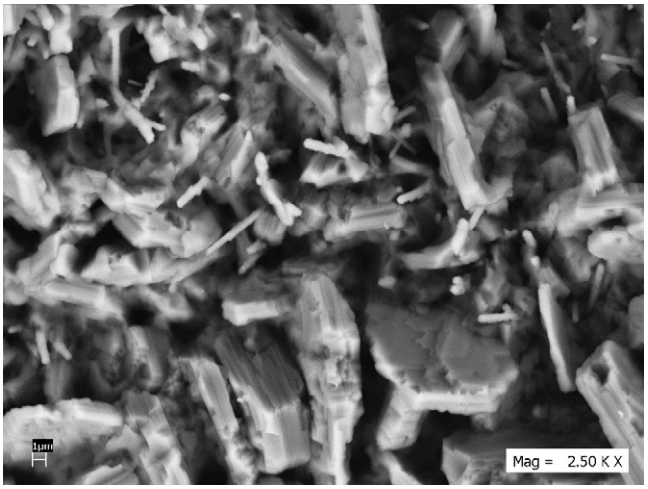

Fig. 13. SEM micrograph of surface of $LaVO_3$ compound into a pellet topology at 850 °C during 15 days prepared by SSR.

Table 2
Global EDX of $LaVO_4$ compound.

Element	% measured	% expected
Sol–gel acrylamide		
La	14.25	15.00
V	15.31	15.00
O	69.94	70.00
Solid state reaction		
La	13.84	15.00
V	15.58	15.00
O	70.58	70.00

Table 3
Global EDX of $LaVO_3$ compound.

Element	% measured	% expected
Sol–gel acrylamide		
La	18.16	20.00
V	18.46	20.00
O	63.38	60.00
Solid state reaction		
La	18.68	20.00
V	18.82	20.00
O	62.50	60.00

of each pellet. One finds higher oxygen concentration at the end of the synthesis in both samples. It is probably due to the oxygen absorption from the atmosphere.

Table 3 shows the global EDX results for $LaVO_3$ compound prepared by SGAP and SSR. The percentage concentrations of cations La and V in the $LaVO_3$ compound determined by this technique are in agreement with those obtained by stoichiometry analysis. This behaviour was observed for both samples. Limited evidence of Zr (0.23%) and Si (0.11%) presence was confirmed by this technique, even though these could not be detected by XRD.

4.4.4. Transmission electron microscopy

An image from transmission electron microscopy study for $LaVO_3$ is shown in Fig. 14. It was indexed as the [1 0 1] zone axe with an orthorhombic Bravais lattice. The particle size by SGAP determined is 43 nm and SSR is 600 nm. This is in agreement with the XRD results. Respect to the morphology this results is in agreement with AFM and SEM results for sample prepared by SGPA. The obtained lattice parameters were: $a = 5.5518$ Å, $b = 7.8480$ Å and $c = 5.5540$ Å with a c/a ratio about 1.00. The planes and the angle between planes are shown in Table 4. The same results were found in the sample prepared by SSR.

4.4.5. Fourier transform infrared spectroscopy

The infrared spectra (Fig. 15) of xerogel, nanocrystal m-$LaVO_4$ compound and $LaVO_3$ compound show that three main changes occurred; the wave numbers of the absorptions lowered gradually; the band numbers and the bandwidths decreased gradually.

Since the V–O bond in amorphous state is not limited by crystal lattice, the V–O distance gets longer and it is non uniform, thus causing the band to broaden. There are bands in the 3680–2800 cm^{-1}

Table 4
Planes and angle between planes obtained in the TEM micrograph powders of $LaVO_3$ prepared by SGAP.

Plane	Plane	Angle between planes (°) ± 0.05
(1 0 $\bar{1}$)	(1 1 $\bar{1}$)	26.0
(0 2 0)	(1 1 $\bar{1}$)	64.0
(0 2 0)	(1 2 $\bar{1}$)	46.5
(0 2 0)	(1 0 $\bar{1}$)	90.0

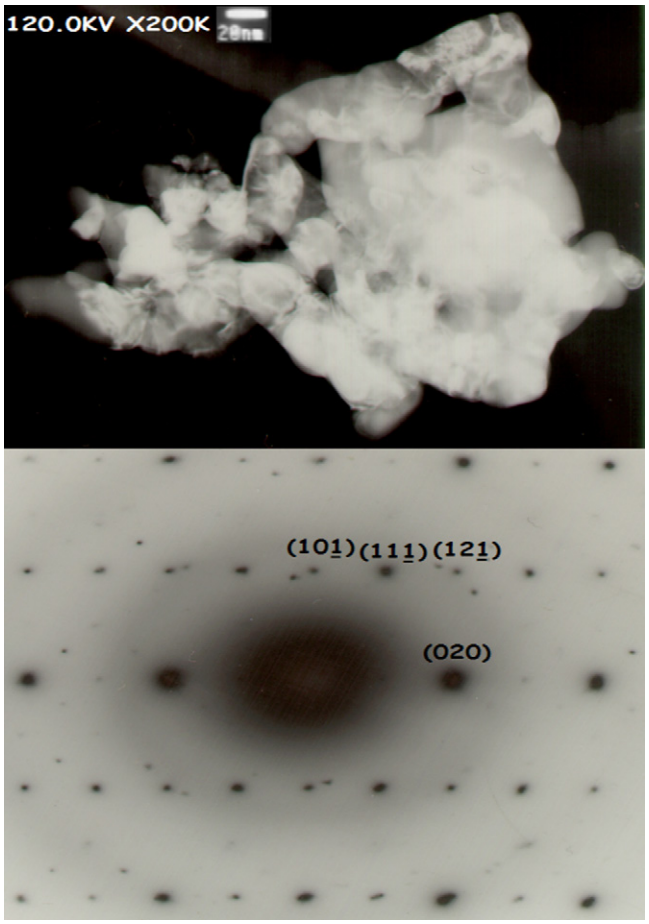

Fig. 14. TEM micrograph powders of $LaVO_3$ compound prepared by SGAP and indexed diffraction pattern of [1 0 1] zone axe.

and the 1800–1140 cm^{-1} regions that correspond to C–H, C–O, O–H and nitrate stretching bond vibration [74–76]. The band in the region from 1015 cm^{-1} to 1040 cm^{-1} is the vibrational mode of isolated V=O bonds in vanadium pentaoxide [77]. The band centered at 822 cm^{-1} can be attributed to ν(V–O–V) vibration polymeric vanadates [78].

The spectrum of the heat treatment m-$LaVO_4$ powders shows that the bands in the 3640–2990 cm^{-1} and 1780–1150 cm^{-1} regions remain and the other absorptions decrease when the $LaVO_4$ crystalline phase starts to form at 400 °C. The absorption band at 1385 cm^{-1} is the bending mode of OH, which results from absorption of H_2O on La_2O_3 because the milled La_2O_3 sample has strong tendency to absorb moisture to form hydroxide during sample handling [79]. Also, one can observe how the absorption shoulder at 1025 cm^{-1} is attributed to the presence of V_2O_5. The peaks at 771, 804, 825, 859, 880 and 898 cm^{-1} are attributed to the formation of $LaVO_4$ [79–82].

The spectrum obtained for $LaVO_3$ powders after the heat treatment of 850 °C shows the decrease of the broad band at lower wave numbers (below 2000 cm^{-1}). This change in the V=O band length in the spectrum is attributed to the changing of coordination number of vanadium due to the formation of $LaVO_3$ compound. The pres-

Table 5
Infrared shifts of rare earth vanadates in cm^{-1} prepared by SGAP.

Composition	V_2O_5	ν(V=O)	ν(V=O)
$LaVO_4$	1030	804	771
$LaVO_3$	1020	798	759

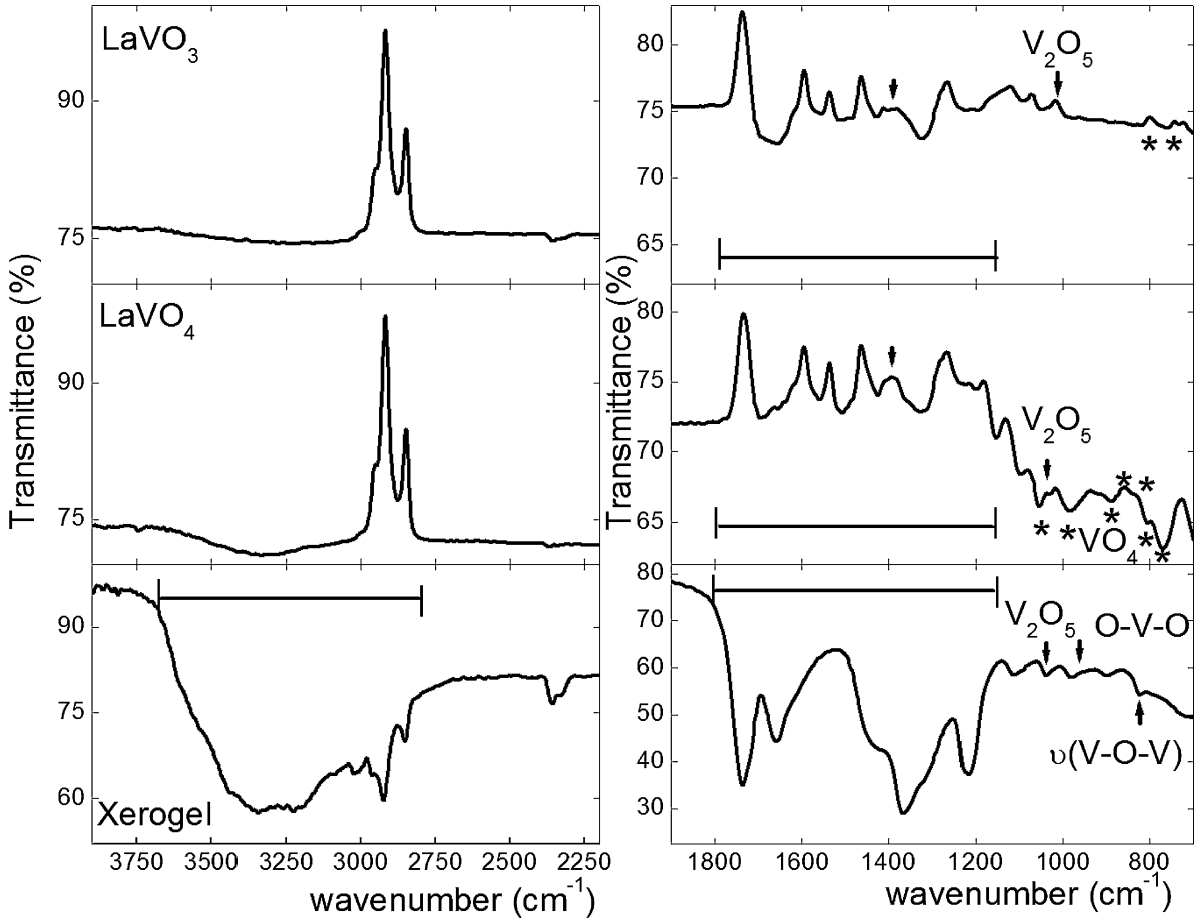

Fig. 15. FT-IR spectra of sample prepared by SGAP at xerogel 100 °C, powders of $LaVO_4$ compound at 400 °C, and powders of $LaVO_3$ compound after 850 °C.

ence of some weak bands located in the interval of 1100–1650 cm^{-1} could be attributable to the absorptions of water and CO_2 from the atmosphere. Table 5 gives the absorption bands for rare earth vanadates.

5. Conclusions

In this work we contrast the production of $LaVO_3$ polycrystalline samples obtained by reduction of the m-$LaVO_4$ prepared by two different methods: sol–gel acrylamide polymerization (SGAP) and solid state reaction (SSR). The sample produced by SGAP shows the formation of m-$LaVO_4$ compound at 400 °C instead of 1400 °C for SSR. The crystal structure of both samples is however the same in both samples. The morphology of $LaVO_4$ compound prepared by SGAP reveals a homogeneous needle-shaped grains in the nanometer range instead of samples obtained by SSR. The morphology of m-$LaVO_4$ compound depends of EDTA molar ratio and pH value. The grain size uniformity follows in the nanometer scale up to the formation of $LaVO_3$ compound prepared by SGAP compared with the samples synthesized by SSR. XRD and TEM results for all samples are in agreement with the phase reported in the literature. The IR spectra show that from amorphous to nanocrystals the absorptions shift to lower wave numbers with degenerating and broadening due to size and crystal effects.

Acknowledgments

Research is supported by grants UNAM-PAPIIT IN109308 and CONACYT U41007-F and 56764.

References

[1] H.C. Nguyen, J.B. Goodenough, Phys. Rev. B 52 (1) (1995) 324–334.
[2] Y. Ren, A.A. Nugroho, A.A. Menovsky, J. Strempfer, U. Rütt, F. Iga, T. Takabatake, C.W. Kimball, Phys. Rev. B 67 (2003) 014107.
[3] J.-Q. Yan, J.-S. Zhou, J.B. Goodenough, Phys. Rev. Lett. 93 (2004) 235901.
[4] M. De Raychaudhury, E. Pavarini, O.K. Andersen, Phys. Rev. Lett. 99 (2007) 126402.
[5] G. Liu, X. Duan, H. Li, H. Dong, L. Zhu, J. Cryst. Growth 310 (2008) 4689–4696.
[6] K. Oka, H. Unoki, H. Shibata, H. Eisaki, J. Cryst. Growth 286 (2006) 288–293.
[7] Y. Oka, T. Yao, N. Yamamoto, J. Solid State Chem. 152 (2000) 486–491.
[8] J.W. Stouwdam, M. Raudsepp, F.C.J.M. Van Veggel, Langmuir 21 (2005) 7003–7008.
[9] E.J. Baran, P.J.Z. Aymonino, Anorg. Allg. Chem. Eizeldarst. 383 (1971) 220 (Powders diffraction file JCPDS 25-427).
[10] C.E. Rice, W. Robinson, Acta Crystallogr. B 32 (1976) 2232.
[11] J. Bashir, M. Nasir Khan, Mater. Lett. 60 (2006) 470–473.
[12] M.R.B. Andreeta, A.S.S. de Camargo, L.A.O. Nunes, A.C. Hernades, J. Cryst. Growth 291 (2006) 117–122.
[13] W. Fan, X. Song, S. Sun, X. Zhao, J. Solid State Chem. 180 (2007) 284–290.
[14] I.V. Solovyev, Phys. Rev. B 74 (2006) 054412.
[15] P. Bordet, C. Chaillout, M. Marezio, Q. Huang, A. Santoro, S.-W. Heong, H. Takagi, C.S. Oglesby, B. Batlogg, J. Solid State Chem. 106 (1993) 253–270.
[16] R.T.A. Kahn, J. Bashir, N. Iqbal, M. Nasir Khan, Mater. Lett. 58 (2004) 1737–1740.
[17] H.C. Nguyen, J.B. Goodenough, J. Solid State Chem. 119 (1995) 24–35.
[18] M. Onoda, H. Nasagawa, Solid State Commun. 99 (7) (1996) 487–491.
[19] A. Masuno, T. Terashima, M. Takano, Solid State Ionics 172 (2004) 275–278.
[20] A.V. Mahajan, D.C. Johnston, D.R. Torgeson, F. Borsa, Phys. Rev. B 46 (1992) 10966.
[21] J. Kikuchi, H. Yasuoka, Y. Kokubo, Y. Ueda, J. Phys. Soc. Jpn. 63 (1994) 3577–3580.
[22] H. Sawada, N. Hamada, K. Terakura, T. Asada, Phys. Rev. B 53 (1996) 12742.
[23] Y. Ren, T.T.M. Palstra, D.I. Khomskii, E. Pellegrin, A.A. Nugroho, A.A. Menovsky, G.A. Sawatzky, Nat. London 396 (1998) 441–444.
[24] S. Miyasaka, Y. Okimoto, Y. Tokura, J. Phys. Soc. Jpn. 71 (9) (2002) 2086–2089.
[25] G. Khaliullin, P. Horsch, A.M. Olés, Phys. Rev. Lett. 86 (2001) 3879–3882.
[26] L.T. Tung, M.R. Lees, G. Balakrishnan, D.M. Paul, Phys. Rev. B 75 (2007) 104404.
[27] Z.M. Fang, Q. Hong, Z.H. Zhou, S.J. Dai, W.Z. Weng, H.L. Wan, Catal. Lett. 61 (1999) 39–44.
[28] C.T. Au, W.D. Zhang, H.L. Wan, Catal. Lett. 37 (1996) 241–246.

[29] P.N. Trikalitis, T.V. Bakas, A.C. Moukarita, A.T. Sdoukos, T. Angelidis, P.J. Pomonis, Appl. Catal. A: Gen. 167 (1998) 295–308.
[30] K.-T. Li, Z.-H. Chi, Appl. Catal. A: Gen. 206 (2001) 197–203.
[31] M. Ross, IEEE J. Quantum Elect. 11 (1975) 938.
[32] L. Zhang, Z. Hu, Z. Lin, G. Wang, J. Cryst. Growth 260 (2004) 460–463.
[33] L.H. Brixner, E. Abramson, J. Electrochem. Soc. 112 (1) (1965) 70–74.
[34] B. Yan, X.-Q. Su, J. Alloys Compd. 431 (2007) 342–347.
[35] W. Fan, Y. Bu, X. Song, S. Sun, X. Zhao, Cryst. Growth Des. 7 (11) (2007) 2361–2366.
[36] Y. Wang, Y. Zuo, H. Gao, Electrochem. Solid-State Lett. 10 (6) (2007) J71–J74.
[37] C.-J. Jia, L.-D. Sun, F. Luo, X.-C. Jiang, L.-H. Wei, C.-H. Yan, Appl. Phys. Lett. 84 (26) (2004) 5305–5307.
[38] F.C. Palilla, A.K. Levine, M. Rinkevics, J. Electrochem. Soc. 112 (8) (1965) 776–779.
[39] R.C. Ropp, J. Electrochem. Soc.: Solid State Sci. 115 (9) (1968) 940–945.
[40] J. Liu, Q. Yao, Y. Li, Appl. Phys. Lett. 88 (2006) 173119.
[41] A. Wold, R. Ward, J. Am. Chem. Soc. 76 (1954) 1096.
[42] A.J. Moulson, J.M. Herbert, Electroceramics Materials Properties Applications, Chapman and Hall, London, 1990.
[43] A. Sin, P. Odier, Adv. Mater. 12 (9) (2000) 649–652.
[44] A. Douy, P. Odier, Mater. Res. Bull. 24 (1992) 1119.
[45] A. Sin, P. Odier, F. Weiss, M. Nuñez-Regueiro, Physica C 341–348 (2000) 2459–2460.
[46] A. Douy, Inorg. Mater. 3 (7) (2001) 699–707.
[47] A. Calleja, X. Casas, I.G. Serradilla, M. Segarra, A. Sin, P. Odier, F. Espiell, Physica C 372–376 (2002) 1115.
[48] A. Sin, B. El Montaser, P. Odier, J. Sol–Gel Sci. Technol. 26 (2003) 541–545.
[49] G. Herrera, E. Chavira, J. Jiménez-Mier, L. Baños, J. Guzmán, C. Flores, J. Sol–Gel Sci. Technol. 46 (2008) 1.
[50] Y. Song, C.-W. Nan, J. Sol–Gel Sci. Technol. 44 (2007) 139–144.
[51] S. Francis, L. Varshney, Radiat. Phys. Chem. 74 (2005) 310–316.
[52] C. Escudero, C. Gabaldón, P. Marzal, I. Villaescusa, J. Hazard. Mater. 152 (2008) 476–485.
[53] I. Puigdomenech, Inorganic Chemistry Royal Institute of Technology Stockholm, Sweden HYDRA and MEDUSA software download from http://www.kemi.kth.se/medusa.
[54] S.A. Brandán, A. Ben Altabef, E.L. Varetti, Spectrochim. Acta 51 (4) (1995) 669–675.
[55] N. Logan, Pure Appl. Chem. 58 (8) (1986) 1147–1152.
[56] H. Seim, H. Fjelvag, B.C. Hauback, Acta Chem. Scand. 52 (1998) 1301.
[57] R. Pankajavalli, O.M. Sreedharan, Mater. Lett. 24 (1995) 247–251.
[58] K. Kitayama, D. Zoshima, T. Katsura, Bull. Chem. Soc. Jpn. 56 (3) (1983) 689–694.
[59] O. Kubachewski, C.B. Alcock, Metallurgical Thermochemistry, 5th ed., Pergamon Press, Oxford, 1983.
[60] R.B. Leane, WinSPM DPS ©version 2.00 JEOL Ltd., 1989–2002.
[61] Universal Analysis 2000 ©version 4405 TA Instruments Waters LLC, 1998–2006.
[62] Spectrum ©version 5.0.1 Perkin Elmer Instruments LLC, 2003.
[63] K. Daimon, W. Min, Y. Hikichi, N. Wada, T. Matsubara, T. Ota, Chem. Soc. Jpn. 3 (2003) 455–458.
[64] H. Wu, H. Xu, Q. Su, T. Chen, M. Wu, J. Mater. Chem. 13 (2003) 1223.
[65] J. Liu, Y. Li, J. Mater. Chem. 17 (2007) 1797–1803.
[66] W. Fan, X. Song, Y. Bu, S. Sun, X. Zhao, J. Phys. Chem. B 110 (46) (2006) 23247–23254.
[67] C. Jia, L. Sun, L. You, X. Jiang, F. Luo, Y. Pang, C. Yan, J. Phys. Chem. B 109 (2005) 3284–3290.
[68] R.C. Weast (Ed.), CRC Handbook of Chemistry and Physics, 1st Student ed., CRC Press, Boca Raton, FL, 1988, B-76.
[69] A.I. Fernández, A. Calleja, J.M. Chimenos, M.A. Fernández, X.G. Capdevila, M. Segarra, H. Xuriguera, F. Espiell, J. Sol–Gel Sci. Technol. 36 (2005) 11–17.
[70] K.J. Rao, B. Vidhyanathan, M. Ganguli, P.A. Ramakrishnan, Chem. Mater. 11 (4) (1999) 882–895.
[71] A. Watanabe, National Inst. for Inorganic Materiales, Tsukuba, Japan, 1999.
[72] P. Schols, Carnoy ©version 2.0 Laboratory of Plant Systematics, Katholieke Universiteit Leuven, 2001.
[73] Microcal Origin ©version 6.0 Microcal Software, Inc., 1991–1999.
[74] K.A. Rubinson, J.F. Rubinson, Análisis Instrumental, Pearson Educación, S.A., Madrid, 2001.
[75] H. Zhang, X. Fu, S. Niu, G. Sun, Q. Xin, J. Solid State Chem. 177 (2004) 2649–2654.
[76] M. Yu, J. Lin, Z. Wang, J. Fu, S. Wang, H.J. Zhang, Y.C. Han, Chem. Mater. 14 (2002) 2224–2231.
[77] R. Ceccato, G. Carturan, F. Decker, F. Artuso, J. Sol–Gel Sci. Technol. 26 (2003) 1071–1074.
[78] C.B. Rodella, R.W.A. Franco, C.J. Magon, J.P. Donoso, L.A.O. Nunes, M.J. Saeki, M.A. Aegerter, V. Sargentelli, A.O. Florentino, J. Sol–Gel Sci. Technol. 25 (2002) 83–88.
[79] T. Tojo, Q. Zhang, F. Saito, J. Alloys Compd. 427 (2007) 219–222.
[80] E. Antic-Fidancev, J. Hölsa, M. Lemaitre-Blaise, P. Porcher, J. Phys.: Condens. Matter 3 (1991) 6829–6843.
[81] S. Varma, B.N. Wani, N.M. Gupta, Appl. Catal. A: Gen. 205 (2001) 295–304.
[82] S. Varma, B.N. Wani, N.M. Gupta, Mater. Res. Bull. 37 (2002) 2117–2127.